Cryogenics 142 (2024) 103895

Contents lists available at ScienceDirect

Cryogenics

journal homepage: www.elsevier.com/locate/cryogenics

Characterizing 1550 nm optical components down to 8 K

Tim J. Kuhlbusch [a,*,1], Morgane Zeoli [b,c,1], Robert Joppe [a], Christophe Collette [c], Thomas Hebbeker [a], Joris V. van Heijningen [b,d,e], Achim Stahl [a]

[a] III. Physikalisches Institut, RWTH Aachen University, Otto-Blumenthal-Straße, 52074, Aachen, Germany
[b] Centre for Cosmology, Particle Physics and Phenomenology (CP3), UCLouvain, Chemin du Cyclotron 2, B-1348, Louvain-la-Neuve, Belgium
[c] Precision Mechatronics Laboratory, ULiège, B52/Quartier Polytec 1, B-4000, Liège, Belgium
[d] Department of Physics and Astronomy, VU Amsterdam, De Boelelaan 1081, 1081 HV Amsterdam, the Netherlands
[e] Nikhef, Science Park 105, 1098 XG Amsterdam, the Netherlands

ARTICLE INFO

Keywords:
Photodiodes
Cryogenics
Optics
1550 nm optics
Collimator
Interferometric sensing
Extended InGaAs
Gravitational wave detection

ABSTRACT

Thermal noise sources are relevant for future gravitational wave detectors due to the foreseen increase in sensitivity, especially at frequencies below 10 Hz. As most thermal noise sources scale with the square root of the temperature, cooling critical optical components and their suspension system is essential. This also requires a much wider range of temperature compatibility from all technology deployed in the last suspension stages, including displacement and inertial sensors. We demonstrate and characterize a setup for stable light sources and light intensity sensing for temperatures from 300 to 12 K. Commercial collimators and fibers were tested to use light from stabilized laser sources in the cryogenic environment. We also investigated multiple semiconductor compositions of photodiodes and identified a solution with high and stable responsivity at 1550 nm.

1. Introduction

Over the past decade, several ground-based observatories have been operating to capture gravitational waves. Current instruments can detect gravitational-wave signals with frequencies higher than 10 Hz [1,2]. They are limited at low frequency by multiple noise sources, including the coupling of the mirror motion with other degrees of freedom, seismic noise, and thermal noise. The Einstein Telescope is a third-generation gravitational wave detector. The project aims at increasing the observable fraction of the Universe by broadening the frequency range of observation down to 3 Hz and increasing the sensitivity [3]. As most thermal noise contributions scale with the square root of the temperature, the main sources of thermal noise, the mirror coatings and mirror suspensions, will be cooled to between 10 and 20 K. With improved seismic isolation systems, noise from ground vibrations is expected to be reduced to non-limiting levels in the frequency range of interest.

E-TEST (Einstein Telescope Euregio Meuse-Rhine Site & Technology) [4][2] is an international collaboration researching key technologies for the Einstein Telescope [6]. In this context, a prototype suspension is being developed, combining passive and active isolation techniques for a 100 kg silicon mirror cooled down radiatively below 25 K in a suspended cryostat.

The seismic isolation calls for highly sensitive inertial sensors at each stage of the isolation chain to monitor its efficiency. This is especially relevant to characterize the effectiveness of the low-vibration cooling strategy. The sensors close to the mirror must be capable of operating in harsh cryogenic environments with extremely high sensitivity. Horizontal and vertical cryogenic inertial sensors were developed to monitor the cryogenic penultimate stage down to 10^{-13} m/$\sqrt{\text{Hz}}$ and 10^{-14} m/$\sqrt{\text{Hz}}$ respectively below 10 Hz. Interferometric readouts are the state-of-the-art strategy for sub-picometer sensitive sensors [7–11]. However, their compatibility with cryogenic temperature has not been well documented yet. Most of the optical components specifications are stated at room temperature, and their performance at cryogenic temperature needs to be characterized to ensure a reliable operation at cryogenic temperature. The horizontal sensor developed for the last isolation stage of the E-TEST prototype is shown as an example of a cryogenic interferometric inertial sensor in Fig. 1.

In this paper, the compatibility and performance of the critical optical elements of an interferometric readout are investigated under cryogenic conditions. Commercial collimators and polarization-maintaining

* Corresponding author.
E-mail address: kuhlbusch@physik.rwth-aachen.de (T.J. Kuhlbusch).
[1] Both marked authors have an equal contribution to this paper; the order is determined alphabetically.
[2] Additional information can be found in the design report [5].

https://doi.org/10.1016/j.cryogenics.2024.103895
Received 4 June 2024; Received in revised form 4 July 2024; Accepted 13 July 2024
Available online 18 July 2024

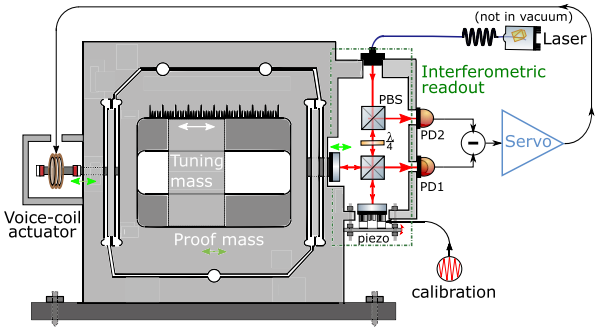

Fig. 1. Concept of a cryogenic monolithic inertial sensor. A homodyne interferometric readout provides an error signal containing information on the position of the proof mass. The proof mass is inertially suspended from the frame by a regular pendulum and inverted pendulum (a Watt's linkage) and allows for an arbitrarily low natural frequency, thereby increasing the mechanical sensitivity. The error signal is fed to the magnet voice-coil actuator to lock the mass with respect to the frame and is used as the sensor output [12]. The interferometer output and feedback control are performed by a custom analog circuit. It is foreseen to replace the analog circuit with a custom Cryo-CMOS chip [13,14].

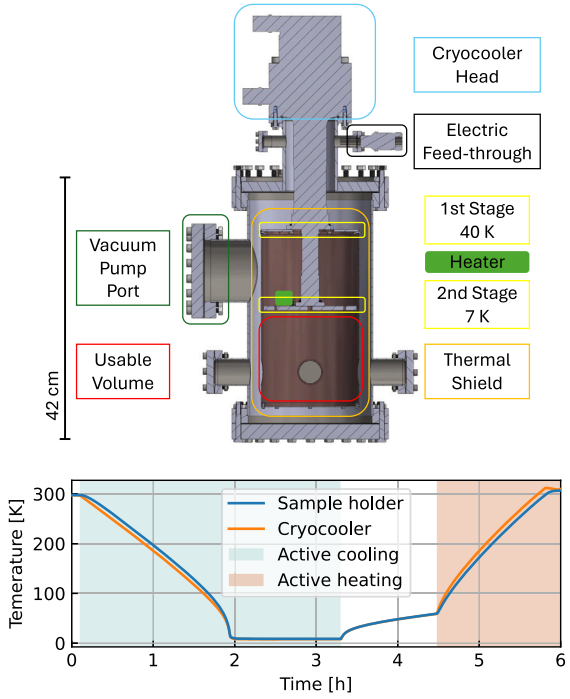

Fig. 2. Top: Cross section of the cryostat used to test optical components. Depicted are the outer stainless steel vessel, cryocooler, thermal shield, and the connection port for the vacuum pump. Bottom: Typical temperature profile during a measurement. The system reaches the minimal temperature after about 2 h of cooling. Once the cooler is stopped, the system starts to heat up slowly. A heater is used to bring the system back to room temperature within a few hours instead of days.

single-mode fibers are tested to use light from stabilized laser sources in the cryogenic environment. Multiple photodiode compositions are investigated as well to select the optimal solution for 1550 nm interferometric readouts.

2. Cryogenic test bench

A closed-cycle cryostat system was used to evaluate components at temperatures between 8 and 300 K and is shown in Fig. 2. The two-stage Gifford-McMahon cooler can cool the system to below 10 K. With a turbomolecular pump the outer stainless steel vessel is evacuated below 1×10^{-5} hPa. The setup is capable of achieving a temperature of 10 K with an additional heat load of 2 W, which is well below the expected heat load of the tested components. After cooling, the temperature of the cold head is stable to within 0.2 K, limited by the cyclic nature of the cooling process. Due to the thermal resistance, the temperatures of the tested devices are even more stable. The setup typically takes 2 h to cool below 10 K and can be actively heated to room temperature within 2 h [4].

3. Collimators

3.1. Material and methods

Sensitive interferometric read-out systems require a stable optical light source. Laser light sources with sufficient stability are commercially available. Fiber splitters can be employed to operate multiple sensors from a single light source. This way, a single fiber entering the cryogenic environment can supply light for multiple devices. Due to their small diameter, single-mode fibers are not very stiff and have lower mechanical coupling compared to their multi-mode counterpart and lower thermal conductivity. Using polarization-maintaining fibers eliminates the need for an additional polarizer that would discard half of the transferred power. Thus, for gravitational-wave detectors, polarization-maintaining single-mode fibers are a practical solution to make this light available in the cryogenic environment. The laser wavelength of interest is 1550 nm. This choice results from the compromise of having a large wavelength to broaden the measurement range of the interferometer [11] and the commercial availability of long-wavelength lasers with low intensity noise and low frequency noise.

Parallel light beams are crucial for the alignment in optical sensors and for all following cryogenic measurements, but bare fiber ends emit light in a divergent pattern. Collimators are used to refract the light into a parallel beam. Therefore two collimators were selected and studied: The F230APC-1550 from Thorlabs was chosen, as fixed-focus collimators from the same family have already been widely used in interferometric readouts [11,15–17]. As a more compact alternative, the CFP5-1550A by Thorlabs was evaluated.

The CFP5 collimator has an integrated fiber with a polymer-based coating (TPE-E) that suggests a high outgassing rate. The F230APC, on the other hand, is primarily made of stainless steel, suggesting that it will have a comparatively low outgassing rate.

The setup shown in Fig. 3 was used to measure the effect of cryogenic temperatures on the collimators. The previously described cryostat system was used to cool the samples at ambient pressures below 1×10^{-6} hPa. Light from a Koheras Adjustik X15 1550 nm laser was coupled into the vacuum vessel of the cryostat using polarization maintaining optical fibers with FC-APC connectors (Thorlabs P3-1550PM-FC). The light throughput between two collimators is sensitive to the angular alignment. To avoid misalignment due to thermal contraction, a 200 µm multi-mode fiber end is used to collect light from the device under test. This solution has a lower light throughput but has a significantly reduced sensitivity to angular misalignment due to the larger numerical aperture of the fiber end. To quantify the output light intensity, the photocurrent of an FGA21 photodiode placed outside of the cryostat was monitored.

Operating the optical fibers outside of their specified temperature range could lead to damage from increased mechanical stress. This is especially true for the unprotected surfaces inside the connectors if dust particles are stuck between the two surfaces. As soon as any degradation to the fiber ends was observed under a microscope, the fibers were replaced to prevent such effects from affecting the measurements.

3.2. Results and discussion

Results from the collimator measurements are summarized in Fig. 4. Both collimators showed no damage or permanent degradation from

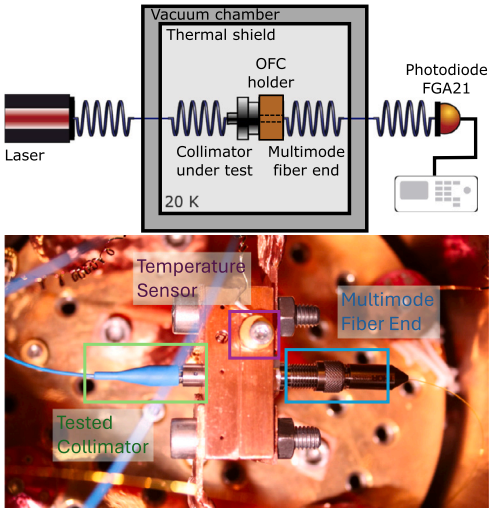

Fig. 3. Top: Sketch of the experimental setup used for collimator testing. Optical fibers are used to couple light into and out of the cryogenic environment. A mounting structure made of oxygen-free copper (OFC) is used to mount an open multi-mode fiber end in front of the collimator and to thermally connect the collimator to the cooling system. Bottom: Picture showing the mounting system for the CFP5 collimator. The mounting structure temperature is measured with a DT-670 temperature sensor by Lake Shore.

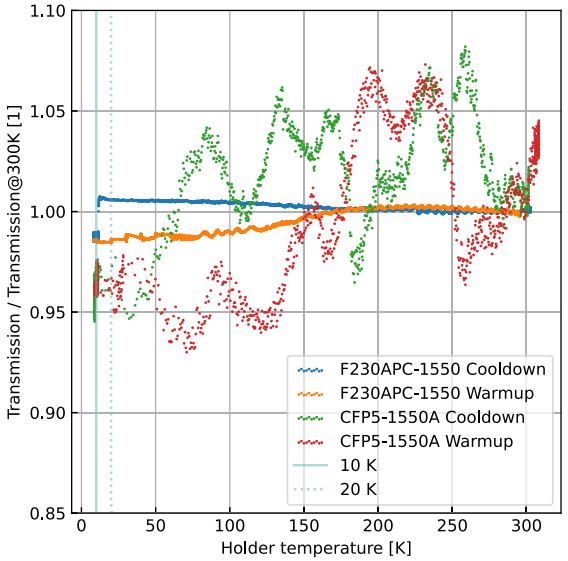

Fig. 4. Measurement of the temperature dependency of the light transmission for the optical system of collimator and fibers. Each shown measurement displays data from a thermal cycle similar to Fig. 2. The CFP5-1550 showed significantly more fluctuations during the cooling cycle compared to the F230APC. Compared to during the temperature ramping, the F230APC had a significantly more stable light throughput at a constant temperature.

the cryogenic temperature. For both collimators, the transmission coefficient stabilized once the temperature stabilized.

The CFP5 collimator transmission varied by about ±7% during cooling and heating. In multiple thermal cycles the amplitude of the variations was repeatable, but the exact shape varied. This could be due to the internal structure of the collimator or caused by movement of the collimator in the mounting structure. The CFP5 has a cylindrical outer shape with one flat side. The used mounting structure had a matching hole with a grub screw. With differences in thermal contraction, the collimator might be able to tilt as the temperature drops. This suggests that a more elaborate mounting solution would be required to apply the CFP5 for precise sensing applications at cryogenic temperatures.

The F230APC collimator has a significantly more stable transmission that varies less than ±2% across the studied temperature range. With an outer thread, the F230APC is much easier to mount. In Fig. 4 the temperature of the holding structure is shown. It is logical that the temperature of the less thermally conductive lens is delayed relative to the holding structure temperature, leading to a difference between the measurements from cool-down and warm-up. The variation in the light between thermal cycles was studied in a combined setup where the sensing photodiode was cooled simultaneously. A maximum variation related to the collimator of 1% was observed.

There are multiple possible reasons for the ±2% variation in light throughput, including the fast change of the F230APC around 10 K.

Residual gasses could form ice layers on the optical surfaces. The ice layer formation rate can be estimated as

$$\eta \approx \frac{P}{\rho_{\text{coating}}} \sqrt{\frac{m}{2\pi k_B T}}, \tag{1}$$

where P is the pressure, ρ_{coating} is the density of the ice layer, m is the mass of the ice molecules, k_B is the Boltzmann constant, and T the temperature of the residual gas [18,19]. This assumes that all molecules incident on the mirror stick to the surface. For the collimator experiments with the largest pressure of up to 1×10^{-6} hPa, water vapor is dominating. Assuming a density $\rho_{\text{coating}} = 0.82\,\text{g/cm}^3$ [20] for light amorphous ice yields an ice growth rate of $\eta \approx 47\,\text{nm/h}$ for residual gas coming from the room temperature outer vacuum vessel. Due to the experiment geometry, most of the residual gas molecules are expected to freeze on other surfaces that are cooled faster, making this an upper-limit estimate. The ice layer formed over the duration of a few hours per experiment is thus thin compared to the wavelength of 1550 nm. Due to this upper limit it is unlikely that ice formation is the dominant reason for variation in the light throughput. The estimation of the ice-layer formation rate presented here is only an upper limit and is specific to our setup. Another possible reason is thermal contraction, which could affect the optical coatings on the collimator lens or lead to deformation of the lens.

Due to the better performance with the employed mounting systems the F230APC is used in all following measurements.

4. Photodiodes

Measuring the power of light beams in cryogenic environments is crucial in constructing cryogenic optical displacement and interferometric inertial sensors. With working collimators and optical fibers, it is possible to guide the light outside the cryogenic environment and use room temperature components. However, this requires at least one fiber per readout channel. In the context of a gravitational-wave detector, each fiber adds undesirable mechanical coupling. The optical output signals of the interferometric readout systems are low-power and sensitive, meaning that disturbances collected over longer distances can decrease the signal-to-noise ratio. In addition, for thermal design reasons, the optical fibers have to be small in diameter, which makes them very fragile. Placing photoelectric sensors like photodiodes directly in the cold environment allows using electrical wiring instead of optical fibers but necessitates photodiodes compatible with the required cryogenic temperatures.

Photodiodes are made of semiconductor junctions and produce an illumination-dependent photocurrent. Several figures of merit are commonly used to describe photodetectors and photodiodes. Among the main ones are the spectral response, the quantum efficiency, the responsivity, and noise level [21]. The spectral response of a photodiode relates to the variation of responsivity with wavelength and is commonly used to refer to the range of the electromagnetic spectrum in which the photodiode is sensitive. This article focuses on 1550 nm, setting a first requirement for the photodiode selection. The photodiode responsivity R (photocurrent per illumination power) typically increases linearly with

the incident photon wavelength λ up to the cut-off wavelength λ_{max}. As photon energies E_γ higher than the band gap energy E_g of the semiconductor material are required to excite electrons from the valence band to the conduction band, the maximum sensitive wavelength can be estimated as

$$E_\gamma = \frac{hc}{\lambda} \geq E_g \Rightarrow \lambda_{max} = \frac{hc}{E_{\gamma_{min}}} = \frac{hc}{E_g}. \quad (2)$$

When the photodiode temperature decreases, the band gap energy increases [22,23]. Therefore, the cutoff wavelength decreases, reducing the spectral range. The responsivity of a photodiode is the detected signal output per watt of incident optical power. It is proportional to the photon wavelength for ideal photodiodes due to the reciprocal relationship between wavelength and photon energy. The responsivity of an optimal photodiode can be expressed as a function of the quantum efficiency η [24] as

$$R = \frac{I_{PD}}{P_{light}} \approx \frac{e\lambda\eta}{hc}, \quad (3)$$

where I_{PD} is the photocurrent of the diode, P_{light} is the incident light power on the sensitive area and e is the elementary charge.

The performance of an inertial sensor is characterized by its noise floor, in which the photodiodes of the interferometric read-out can have a dominant contribution. The noise floor of a sensor is the sum of the shot noise, the dark current noise, and the thermoelectrical and flicker noise from the electronics used to convert the photodiode current into voltage [11,25]. Shot noise relates to the statistical nature of photon beams and manifests as uncertainty in the arrival times of the photons on the photodiode. Since it is directly related to the amplitude of the photocurrent, it will not significantly change with temperature as long as the light source and diode responsivity are sufficiently stable. As the electronics can be placed outside of the cryogenic environment, their noise is not affected by temperature either. The dark current is the electrical current measured on the detector when it is not illuminated. The dark current is composed of thermally produced charge carriers [26,11,25,24]. Temperature and bias voltage are the main dependencies for the dark current.

In this study, the figures of merit of several photodiodes are monitored when the photodiode is cooled from room temperature to 12 K. The responsivity of the photodiode is quantified by measuring the produced current under constant illumination. Monitoring the responsivity is also an indication of the spectral range evolution with temperature. The dark current is monitored in separate measurements without illumination, as it is a limiting factor in the interferometric read-out sensitivity.

4.1. Diode selection

In the near-infrared range of the electromagnetic spectrum, more specifically at 1550 nm, only a few commercially available semiconductor-based photodetectors are sensitive: InGaAs, HgCdTe, InAs, and PbS [21,24,27,23,28]. HgCdTe diodes are sensitive up to 13 µm and have a wide energy gap semiconductor CdTe with a semi-metallic compound HgTe [21]. The semiconductor band gap can be tuned by modifying the HgTe and CdTe proportions. The fabrication process of such material is challenging, leading to consequent pricing and uncertainty in the cut-off frequency [23,29,30]. HgCdTe-based photodiodes are thus not considered in this study. PbS-based pin photodiodes are not considered either because of their limited availability in the market.

Using a substrate with a matching lattice constant is a common technique to reduce faults in semiconductor crystals. Lattice-matched InGaAs (typically $In_{0.53}Ga_{0.47}As$ [31]) is the state-of-the-art solution for room temperature 1550 nm detection. Their cutoff wavelength is 1.7 µm and their peak sensitivity is at 1550 nm. However, according to previous studies, the cutoff wavelength is expected to decrease to 1546.3 nm at 20 K due to the increasing band gap energy [22], cutting the current working wavelength out of the spectrum range. To tackle the sensitivity loss of InGaAs with temperature, extended InGaAs photodiodes are considered. Extended InGaAs have an increased Indium content. The band gap equivalent cut-off wavelength at room temperature can vary between 870 nm for pure GaAs and 3500 nm for InAs [27]. Extended InGaAs materials are convenient because of the flexibility in the choice of the cutoff wavelength but are more difficult to manufacture [22,30] compared to lattice-matched systems. The lattice mismatch leads to a smaller bandgap, and the interface defects resulting from the lattice mismatch of extended InGaAs photodiodes lead to higher dark currents [27,32].

Table 1 gives an overview of the different photodiode semiconductor systems considered in this study. Transistor Outline (TO) type packages (e.g. TO-46 [33]) were selected for all diodes for two reasons. First, the mostly metallic packaging promises reduced outgassing rates compared to packages with more exposed potting compound. Additionally, the metal case provides a better thermal contact between the mounting structure and the die. One disadvantage is that for some commercial diodes, the case is connected to one of the terminals of the diode. This can introduce noise and hinder precise measurements by creating ground loops.

4.2. Methodology for diode characterization

The photodiodes were characterized at cryogenic temperature with and without illumination. A general description of the measurement setup can be seen in Fig. 5. The figure also shows the mounting structure for the photodiodes inside of the cryostat. The fibers and collimators characterized in Section 3 were used to illuminate the device under test with light of constant intensity. The 1550 nm laser source power was set to 1 mW. As demonstrated in the previous section, the variation of light intensity with temperature is less than 2% for this setup. To reduce electronic disturbances, the diode mounting structure shown in Fig. 5 was joined with electrically isolating glue. Unfortunately, creating an electrically isolating connection also limits the thermal conductivity, slightly increasing the lowest achievable temperature.

The stainless steel vacuum vessel of the cryostat is the first layer that blocks external light sources. Additionally, the mounting structure for the diodes is completely enclosing the optical path, except for a small off-axis venting hole.

To characterize the dark current, the illumination was disabled, optical ports were closed and all potential light sources were removed. This included disabling the vacuum gauge. To measure the dark current, a Keithley 6485 picoampere meter was used. A custom battery-powered, adjustable, and stabilized voltage source provided the bias voltage without creating ground loops. All cables were shielded and kept as short as possible to minimize coupling from external noise sources. In a trade-off to reduce the introduction of heat through the electrical wiring, the used wiring setup had a leakage resistance of about 40 GΩ. Changes of the leakage resistance with temperature lead to variations of the leakage current up to 40 pA during thermal cycling, limiting the usable measurement range.

4.3. Results and discussion

4.3.1. Responsivity

Results from the measurement campaign are summarized in Fig. 6. The photodiodes from Table 1 were cooled down to approximatively 10 K, and the evolution of their responsivity to a 1550 nm input wavelength with respect to temperature is analyzed. A previous measurement by Bajpai et al. [34] of the FGA21 photodiode is also included for comparison. In some measurements, a small difference between the cooling and warming phases is evident. This happens mainly because it is only possible to measure the temperature of the holding structure and not the temperature inside the diode housing. As is to be expected based

Table 1
List of the commercial photodiodes that were considered. The diodes were chosen to test different semiconductor compositions. Displayed properties are based on the specifications given by the manufacturer. All studied photodiodes have a sensitive area with 1 mm diameter.

Model name	Manufacturer	Material	Room temperature 50% cutoff wavelength [µm]	Room temperature responsivity at 1.55 µm [A/W]
FGA21	Thorlabs	Lattice-matched InGaAs	1.7	1.04
IG17X1000S4i	Laser Components	Lattice-matched InGaAs	1.65	1.05
IG22X1000S4i	Laser Components	Extended InGaAs	2.15	1.09
IG26X1000S4i	Laser Components	Extended InGaAs	2.45	1.0
P10090-01	Hamamatsu	InAs	3.65	0.3

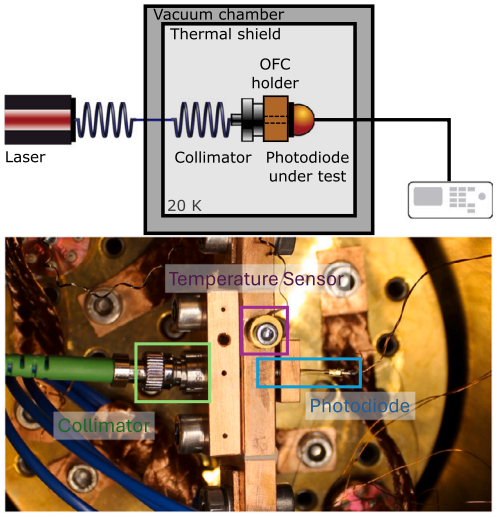

Fig. 5. The setup used for the photodiode characterization: Top: A sketch of the measurement setup where the photodiode is mounted inside the cryogenic environment and illuminated through a single-mode optical fiber and collimator. Bottom: The copper holding structure used to mount the diodes in the cryostat. The structure provides mechanical alignment between the diode and collimator and a good thermal connection.

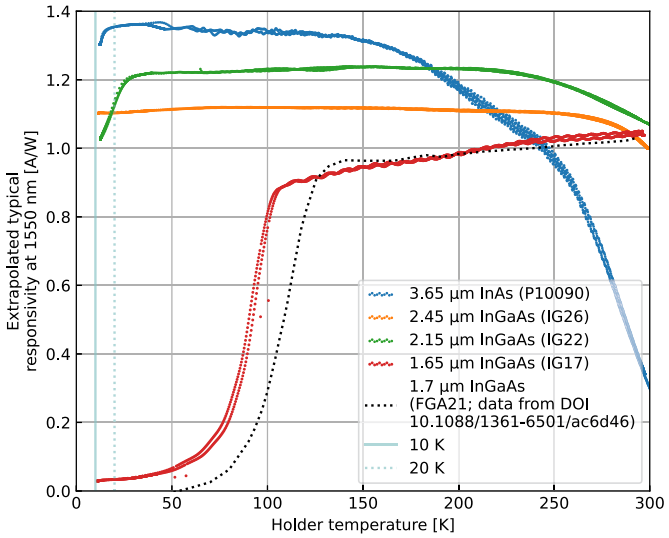

Fig. 6. Measurements of the responsivity of different photodiodes for 1550 nm illumination. All measurements were performed in photovoltaic mode without biasing. A previous measurement by Bajpai et al. [34] of the lattice-matched InGaAs photodiode FGA21 is also included for comparison to our measurements of the lattice-matched InGaAs diode IG17. Each curve displays data from cooling down a photodiode to approximately 10 K and the following warming up. The measurement data is scaled based on the responsivity specified in the respective datasheets at room temperature.

on their lower room temperature maximum wavelength, the lattice-matched 1.65 µm InGaAs diode loses sensitivity to the 1550 nm wavelength at about 93 K (50% loss). This loss was estimated at 84.2 K based on empirical relationships extracted from the literature [22] for lattice-matched InGaAs photodiodes. This experimental result also matches a previous measurement of the FGA21, another lattice-matched InGaAs diode [34], conducted in similar conditions.

All of the extended InGaAs diodes sustain sufficient sensitivity across the whole temperature range. The comparatively low InAs sensitivity at room temperature increases to the highest measured value of about 1.35 A/W. A measurement of the less extended IG22 shows a significant temperature dependency below 30 K. This is disadvantageous for precise sensing applications. A similar effect starting at a lower temperature was observed for the studied InAs diode P10090. Overall, the IG26 displayed the most stable behavior with good responsivity below 20 K. All diodes showed no significant degradation of performance from being thermally cycled twice.

4.3.2. Dark current

The dark current is a bias-dependent current of the photodiode that is present with no illumination of the active area. The current originates from the thermal generation of charge carriers in the depletion region.

The dark current I_D is expected to decrease with decreasing temperature as

$$I_D(T) \approx C \cdot \exp\left(\frac{eV_D - E_g}{nk_BT}\right), \tag{4}$$

where C is a material dependent constant, V_D is voltage applied to the diode, E_g is the bandgap energy, n is the ideality factor and T the temperature [35,36]. For temperature ranges with an insignificant variation of the bandgap energy and ideality factor, a simplification of the exponent is possible and is

$$I_D(T) \approx I_{D,0}\, 2^{T/T_{1/2}}, \tag{5}$$

where $T_{1/2}$ is a parameter in the exponential approximation. We find that for temperatures above 210 K the dark current halves for about every 10 K decrease in temperature. This is a common behavior for most semiconductor junctions and has also been found a good approximation for extended InGaAs around 260 K [37].

Fig. 7 shows the measured dark current for the 1.65 µm and 2.45 µm InGaAs diodes. As the dark current of the two diodes significantly differs, different bias voltages were chosen based on the datasheet recommendations [38,39]. For larger currents, the uncertainty of the picoampere meter calibration is dominant. At temperatures below approximately 100 and 200 K respectively, the uncertainty of the leakage current of the cables limits the measurement, and only an upper bound for the dark current can be given.

The measured dark current values at room temperature are within the specifications given by the manufacturer. A fit with the exponential approximation (5) is shown in Fig. 7. The behavior of both diodes can be well described with the exponential approximation above 200 K. For the

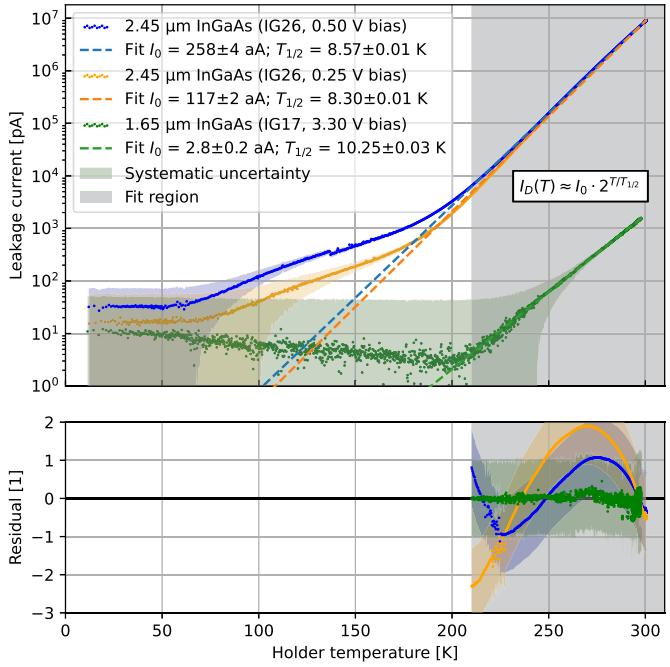

Fig. 7. Temperature dependence of the photodiode dark current. A fit with an exponential model is displayed for the data from each photodiode above 210 K. The systematic errors are dominating for currents below 90 pA and the values are excluded from the fit. For the diode with 2.45 µm cutoff wavelength the simple exponential approximation is not a sufficient model across the studied temperature range. As the cryocooler increases noise to the low current measurements, only data from the warming up period is shown.

1.65 µm cutoff diode, the dark current gets significantly smaller than the measurement uncertainty. Below 200 K, the 2.45 µm diode dark current slope in the semi-log representation significantly differs. This is from multiple effects like the bandgap changing with temperature that the simplified exponential model does not include.

The dark current of the extended InGaAs diode with a cutoff at 2.45 µm dropped by more than five orders of magnitude with decreasing temperature. Below 200 K, the extended (lattice-mismatched) InGaAs diode leakage current is lower than that of the studied lattice-matched diode at room temperature. Therefore, noise performance similar to or better than that of standard InGaAs diodes at room temperature can be reached in small signal applications.

5. Conclusions

As no suitable commercial optical components specified for temperatures below 20 K could be found, promising components for 1550 nm were selected and evaluated. Both tested collimators showed no significant degradation from thermal cycling and had a high light throughput. The F230APC-1550 collimator was selected for further usage as it was more stable with respect to temperature. As the most common lattice-matched InGaAs diodes lose sensitivity for 1550 nm below 100 K, extended InGaAs compositions were investigated. All studied diodes with a room temperature cutoff wavelength above 2 µm maintained a high sensitivity at cryogenic temperatures. A diode with 2.45 µm room temperature cutoff was selected due to good responsivity and temperature stability. At cryogenic temperatures, the comparatively high dark current of the extended InGaAs diodes was significantly reduced, allowing for low noise levels. These findings were used to select optical components that were successfully applied in the E-TEST prototype. This work demonstrates the applicability for cryogenic gravitational-wave detectors like the Einstein Telescope, and other cryogenic optical sensing applications.

This paper focused on injecting and measuring light in a cryogenic environment. The logical continuation is to evaluate the temperature dependency of other critical optical elements such as beam-splitters and other polarization-dependent elements. A detailed verification of a full interferometric sensor is also essential to assess the interplay of the individual components. Evaluating the outgassing rates is another essential step required to employ these components in a gravitational wave detector.

Beyond being used in cryogenic earth-bound gravitational wave detectors, these findings are also relevant in various research fields. Potential applications include interferometric displacement sensors to monitor vibrations in cryostats, cryogenic optical modulators for quantum and cryogenic computing [40], the characterization of cryogenic materials, and space-based applications involving interferometry such as interferometric lunar seismometers [41].

CRediT authorship contribution statement

Tim J. Kuhlbusch: Writing – review & editing, Writing – original draft, Visualization, Validation, Software, Project administration, Methodology, Investigation, Formal analysis, Data curation, Conceptualization. **Morgane Zeoli:** Writing – review & editing, Writing – original draft, Visualization, Validation, Software, Project administration, Methodology, Investigation, Formal analysis, Data curation, Conceptualization. **Robert Joppe:** Resources, Writing – review & editing, Methodology, Conceptualization. **Christophe Collette:** Writing – review & editing, Supervision, Funding acquisition. **Thomas Hebbeker:** Writing – review & editing, Supervision, Funding acquisition. **Joris V. van Heijningen:** Writing – review & editing, Supervision. **Achim Stahl:** Writing – review & editing, Supervision, Funding acquisition.

Declaration of competing interest

The authors declare the following financial interests/personal relationships which may be considered as potential competing interests: All authors report financial support was provided by Interreg V-A Euregio Meuse-Rhine Programme. Morgane Zeoli reports financial support was provided by Fonds National de la Recherche Scientifique (FNRS). If there are other authors, they declare that they have no known competing financial interests or personal relationships that could have appeared to influence the work reported in this paper.

Data availability

Data will be made available on request.

Acknowledgements

This work comes within the scope of the E-TEST project, which is carried out within the framework of the Interreg V-A Euregio Meuse-Rhine Programme, with 7.5 million euros from the European Regional Development Fund (ERDF). By investing EU funds in Interreg projects, the European Union is investing directly in economic development, innovation, territorial development, social inclusion, and education in the Euregio Meuse-Rhine region. Aspects of this work have been previously documented in the internal E-TEST deliverables report. Morgane Zeoli is funded by the Fonds National de la Recherche Scientifique (FNRS) under projet de recherche STELLAR (T.0022.22).

References

[1] The LIGO Scientific Collaboration, Aasi J, Abbott BP, Abbott R, Abbott T, Abernathy MR, Ackley K, et al. Advanced LIGO. Classical and Quantum Gravity 2015;32:074001. https://doi.org/10.1088/0264-9381/32/7/074001.

[2] Acernese F, Agathos M, Agatsuma K, Aisa D, Allemandou N, Allocca A, et al. Advanced Virgo: a second-generation interferometric gravitational wave detector. Classical and Quantum Gravity 2014;32:024001. https://doi.org/10.1088/0264-9381/32/2/024001.

[3] Einstein Telescope Steering Committee Editorial Team, Design report update 2020 for the Einstein Telescope, Technical report, ET-0007B-20. 2020.
[4] Sider A, Fronzo CD, Amez-Droz L, Amorosi A, Badaracco F, Baer P, et al. E-TEST: a compact low-frequency isolator for a large cryogenic mirror. Classical and Quantum Gravity 2023;40:165002. https://doi.org/10.1088/1361-6382/ace230.
[5] Sider A, Amez-Droz L, Amorosi A, Badaracco F, Baer P, Bruno G, et al. E-TEST prototype design report. arXiv:2212.10083, 2022.
[6] Di Pace S, Mangano V, Pierini L, Rezaei A, Hennig J-S, Hennig M, et al. Research facilities for Europe's next generation gravitational-wave detector Einstein telescope. Galaxies 2022;10. https://doi.org/10.3390/galaxies10030065.
[7] Otero J. Development and characterization of an observatory-class, broadband, nonfedback, leaf-spring interferometric seismometer. Ph.D. thesis. San Diego: University of California; 2009.
[8] Collette C, Janssens S, Fernandez-Carmona P, Artoos K, Guinchard M, Hauviller C, et al. Review: inertial sensors for low-frequency seismic vibration measurement. Bulletin of the Seismological Society of America 2012;102:1289–300. https://doi.org/10.1785/0120110223.
[9] van Heijningen JV, Bertolini A, van den Brand JFJ. A novel interferometrically read out inertial sensor for future gravitational wave detectors. In: 2018 IEEE sensors applications symposium (SAS); 2018. p. 1–5.
[10] Zumberge M, Berger J, Otero J, Wielandt E. An optical seismometer without force feedback. Bulletin of the Seismological Society of America 2010;100:598–605. https://doi.org/10.1785/0120090136.
[11] Ding B. Development of high resolution interferometric inertial sensors. Ph.D. thesis. Université Libre de Bruxelles; 2021.
[12] van Heijningen JV. A fifty-fold improvement of thermal noise limited inertial sensitivity by operating at cryogenic temperatures. Journal of Instrumentation 2020;15:P06034. https://doi.org/10.1088/1748-0221/15/06/p06034.
[13] van Heijningen JV, Gatti A, Ferreira EC, Bocchese F, Badaracco F, Lucas S, et al. A cryogenic inertial sensor for terrestrial and lunar gravitational-wave detection. Nuclear Instruments and Methods in Physics Research Section A: Accelerators, Spectrometers, Detectors and Associated Equipment 2022;1041:167231. https://doi.org/10.1016/j.nima.2022.167231.
[14] Tavernier F, Gatti A, Barretto C. Chip design for future gravitational wave detectors. In: 2020 IEEE international electron devices meeting (IEDM); 2020. p. 25.4.1–4...
[15] Watchi J. Active seismic isolation using interferometric inertial sensors. Ph.D. thesis. Université Libre de Bruxelles; 2022.
[16] Cooper SJ. Breaking the seismic wall: how to improve gravitational wave detectors at low frequency. Ph.D. thesis. University of Birmingham; 2019.
[17] Ding B, Zhao G, Watchi J, Sider A, Collette C. An interferometric inertial sensor for low-frequency seismic isolation. Sensors and Actuators A: Physical 2022;335:113398. https://doi.org/10.1016/j.sna.2022.113398.
[18] Labello JM. Water ice films in cryogenic vacuum chambers. Ph.D. thesis. University of Tennessee; 2011.
[19] Hasegawa K, Akutsu T, Kimura N, Saito Y, Suzuki T, Tomaru T, et al. Molecular adsorbed layer formation on cooled mirrors and its impacts on cryogenic gravitational wave telescopes. Phys Rev D 2019;99:022003. https://doi.org/10.1103/PhysRevD.99.022003.
[20] Westley MS, Baratta G, Baragiola R. Density and index of refraction of water ice films vapor deposited at low temperatures. The Journal of chemical physics 1998;108:3321–6.
[21] Abid MM. Spacecraft sensors, space technology library. John Wiley & Sons; 2005. p. 135–203.
[22] Gaskill D, Bottka N, Aina L, Mattingly M. Band-gap determination by photoreflectance of InGaAs and InAlAs lattice matched to InP. Applied physics letters 1990;56:1269–71.
[23] Rogalski A, Antoszewski J, Faraone L. Third-generation infrared photodetector arrays. Journal of Applied Physics 2009;105:091101. https://doi.org/10.1063/1.3099572.
[24] Wertz J, Larson WJ. Space mission analysis and design, space technology library. Dordrecht: Springer; 1999. p. 241–300.
[25] van Heijningen J. Low-frequency performance improvement of seismic attenuation systems and vibration sensors for next generation gravitational wave detectors. Ph.D. thesis. Vrije Universiteit of Amsterdam; 2018.
[26] Perez JV. Multi-band IR sensor for Earth observation. Master Thesis, ULiège. 2019.
[27] Rogalski A. Infrared detectors: status and trends. Progress in Quantum Electronics 2003;27:59–210. https://doi.org/10.1016/S0079-6727(02)00024-1.
[28] Cao F, Liu L, Li L. Short-wave infrared photodetector. Materials Today 2023;62:327–49. https://doi.org/10.1016/j.mattod.2022.11.003.
[29] Rogalski A, Martyniuk P, Kopytko M. Type-ii superlattice photodetectors versus hgcdte photodiodes. Progress in Quantum Electronics 2019;68:100228. https://doi.org/10.1016/j.pquantelec.2019.100228.
[30] Arslan Y, Oguz F, Besikci C. Extended wavelength swir ingaas focal plane array: characteristics and limitations. Infrared Physics & Technology 2015;70:134–7. https://doi.org/10.1016/j.infrared.2014.10.012.
[31] Pearsall T, Hopson R. Growth and characterization of lattice-matched epitaxial films of $Ga_xIn_{1-x}As$/InP by liquid-phase epitaxy. Journal of Electronic Materials 1978;7:133–46.
[32] Martinelli RU, Zamerowski TJ, Longeway PA. 2.6 μm InGaAs photodiodes. Applied Physics Letters 1988;53:989–91. https://doi.org/10.1063/1.100050.
[33] Components Laser. InGaAs-photodiodes package drawings and cooling specifications. https://www.lasercomponents.com/fileadmin/user_upload/home/Datasheets/lc-ingaas/ingaas-photodiodes-package-drawings.pdf, 2021. V04.
[34] Bajpai R, Tomaru T, Yamamoto K, Ushiba T, Kimura N, Suzuki T, et al. A laser interferometer accelerometer for vibration sensitive cryogenic experiments. Measurement Science and Technology 2022;33.
[35] Sze SM, Ng KK. Physics of semiconductor devices. third edition ed. Hoboken, N.J: Wiley-Interscience; 2007.
[36] Shockley W. The theory of p-n junctions in semiconductors and p-n junction transistors. Bell system technical journal 1949;28:435–89.
[37] Li X, Tang H, Li T, Wei P, Gong H, Fang J. Study on dark current of extended wavelength InGaAs detectors. In: Gong H, Shi Z, Chen Q, Lu J, editors. International symposium on photoelectronic detection and imaging 2013: infrared imaging and applications. International society for optics and photonics, vol. 8907. SPIE; 2013. p. 890703.
[38] Components Laser. Regular InGaAs photodiodes IG17-Series. https://www.lasercomponents.com/fileadmin/user_upload/home/Datasheets/lc-ingaas/ig17-regular-ingaas.pdf, 2020. V08.
[39] Laser Components. Extended InGaAs photodiodes IG26-Series. https://www.lasercomponents.com/fileadmin/user_upload/home/Datasheets/lc-ingaas/ig26-extended-ingaas.pdf, 2023. V08.
[40] Eltes F, Villarreal-Garcia GE, Caimi D, Siegwart H, Gentile AA, Hart A, et al. An integrated optical modulator operating at cryogenic temperatures. Nature Materials 2020;19:1164–8. https://doi.org/10.1038/s41563-020-0725-5.
[41] van Heijningen JV, ter Brake HJM, Gerberding O, Chalathadka Subrahmanya S, Harms J, Bian X, et al. The payload of the lunar gravitational-wave antenna. Journal of Applied Physics 2023;133:244501. https://doi.org/10.1063/5.0144687.